



A Stiffness-Tunable Composite with Wide Versatility and Applicability Based on Low-Melting-Point Alloys

Jiawei Xiong¹ · Bo Sun¹ · Chunbao Liu^{1,2} · Konghua Yang¹ · Yuchao Luo¹ · Yunhong Liang^{2,3} · Zhiwu Han² · Lei Ren⁴ · Zhaohua Lin¹

Received: 23 March 2023 / Revised: 3 June 2023 / Accepted: 12 June 2023 / Published online: 4 August 2023
© Jilin University 2023

Abstract

Flexible materials are essential in bionic fields such as soft robots. However, the lack of stiffness limits the mechanical performance of soft robots and makes them difficult to develop in many extreme working conditions, such as lifting and excavation operations. To address this issue, we prepared a stiffness-tunable composite by dispersing low-melting-point alloy into thermosetting epoxy resin. A dramatic and rapid change in stiffness was achieved by changing the state of matter at lower temperatures, and accurate control of the composite modulus was achieved by controlling the temperature. When the alloy content is at 30vol%, the tensile modulus changes 41.6 times, while the compressive modulus changes 58.9 times. By applying the composite to a flexible actuator, the initial stiffness of the actuator was improved by 124 times, reaching 332 mN/mm. In addition, the use of stiffness-tunable materials in the wheel allowed for timely changes in the grounding area to improve friction. These flexible materials with manageable mechanical properties have wide applicability in fields including bionics, robotics, and sensing. Our findings provide a new approach to designing and developing flexible materials with improved stiffness and controllability.

Keywords Stiffness-tunable composite · Manageable mechanical properties · Flexible actuator

1 Introduction

In nature, many organisms adapt to complex and changeable environment by changing their own structural hardness. For example, soft elephant trunks can grasp heavy objects [1], octopuses create virtual joints in the process of movement [2], and sea cucumbers increase the stiffness of the epidermis to protect themselves after being stimulated by the outside world [3]. Inspired by the versatility of these biological

systems, researchers began to design robots with variable stiffness, which can switch reversibly between rigid state and soft state, and change their flexibility and load-bearing capacity. Methods of achieving variable stiffness include building particle-hardened and laminar structures [4–7] (usually by applying vacuum), using shape memory materials [8–12], modulating magnetic field strength to change the stiffness of magnetorheological materials [13, 14], and using gel materials [15–18]. Also, actuating materials are used to induce morphic changes of the load-bearing member so as to result in different stiffness.

Thermally responsive materials can also be used as foundation for variable stiffness structures [19–23]. The softening of such materials is divided into two main cases: melting and glass transition. If the material changes from solid to liquid when heated, the stiffness will be significantly reduced, but liquid leakage must be avoided [24]. Sealing structures clad with low-melting-point metals [18, 25–27] or thermally responsive polymers [16, 28] have been used in variable stiffness systems. For example, Dario Floreano et al. embedded low-melting-point metals in PDMS, which can achieve a 26-fold change in stiffness [24]. Ilse M. Van Meerbeek and

✉ Chunbao Liu
liuchunbao@jlu.edu.cn

Zhaohua Lin
linzhaohua@jlu.edu.cn

¹ School of Mechanical and Aerospace Engineering, Jilin University, Changchun 130022, China

² Key Laboratory of Bionic Engineering, Ministry of Education, Jilin University, Changchun 130022, China

³ Liaoning Academy of Materials, Shenyang 110167, China

⁴ Department of Mechanical, Aerospace and Civil Engineering, University of Manchester, Manchester M139PL, UK

his colleagues prepared silica sponges filled with molten metal, using lost salt method and microfluidic degassing technique to achieve an 18-fold change in tensile modulus [26]. Buckner et al. presented a conductive epoxy resin composite with a 37.2-fold modulus change ratio [20]. Although the reported materials based on thermal response mechanisms have explored the feasibility of stiffness adjustment, they usually suffer from limitations such as small range of stiffness variation, more complex preparation processes and inability to maintain passive deformation. All of these limitations give them a narrow scope of application that cannot combine both versatility and applicability.

In this paper, we provide a simple method for preparation of stiffness-tunable material based on biofunction. A stiffness-tunable composite material with manageable mechanics is prepared by dispersing a low-melting-point alloy into a thermosetting epoxy resin, which is capable of dramatic and rapid changes in stiffness by solid–liquid phase change at lower temperatures. By combining a flexible actuator with variable stiffness materials, we prepared a variable stiffness actuator with the bionic drive concept that deforms under appropriate air pressure. And the deformed state can be passively maintained to carry a maximum load of 800 g. Introducing materials into the design of wheel, the tires is able to switch between soft and hard state at the right time and change its grounding area. The demonstrations illustrate the great potential of using stiffness-tunable materials for bionic drives. The emergence of this variable stiffness material, which can change the direction of deformation by changing the stiffness of the material on the opposite side of the structure, provides more opportunities for the development of traditional pneumatically regulated oscillating class of flexible robots.

2 Material Preparation and Properties

2.1 Material Preparation

In this paper, a new stiffness-tunable composite material is designed by dispersing low-melting-point alloy into thermosetting epoxy resin. In order to prepare the composite, we designed a three-step preparation route, which is simple and fast, as schematically illustrated in Fig. 1a. First, weighing the epoxy resin monomer (EPON828) and curing agent (EPIKURE3164), respectively, in the ratio of 2:1 by mass. Mixing them thoroughly and placing them in a vacuum drier at room temperature for 20 min to remove the mixed air. Subsequently, spherical Bi-In-Sn alloy grains with a diameter of 5 μm are heated at 100 °C to transform them into a molten state. Pouring different masses of alloy in molten state into epoxy resin. The specific proportions between these materials are shown in Table S1 (Supporting

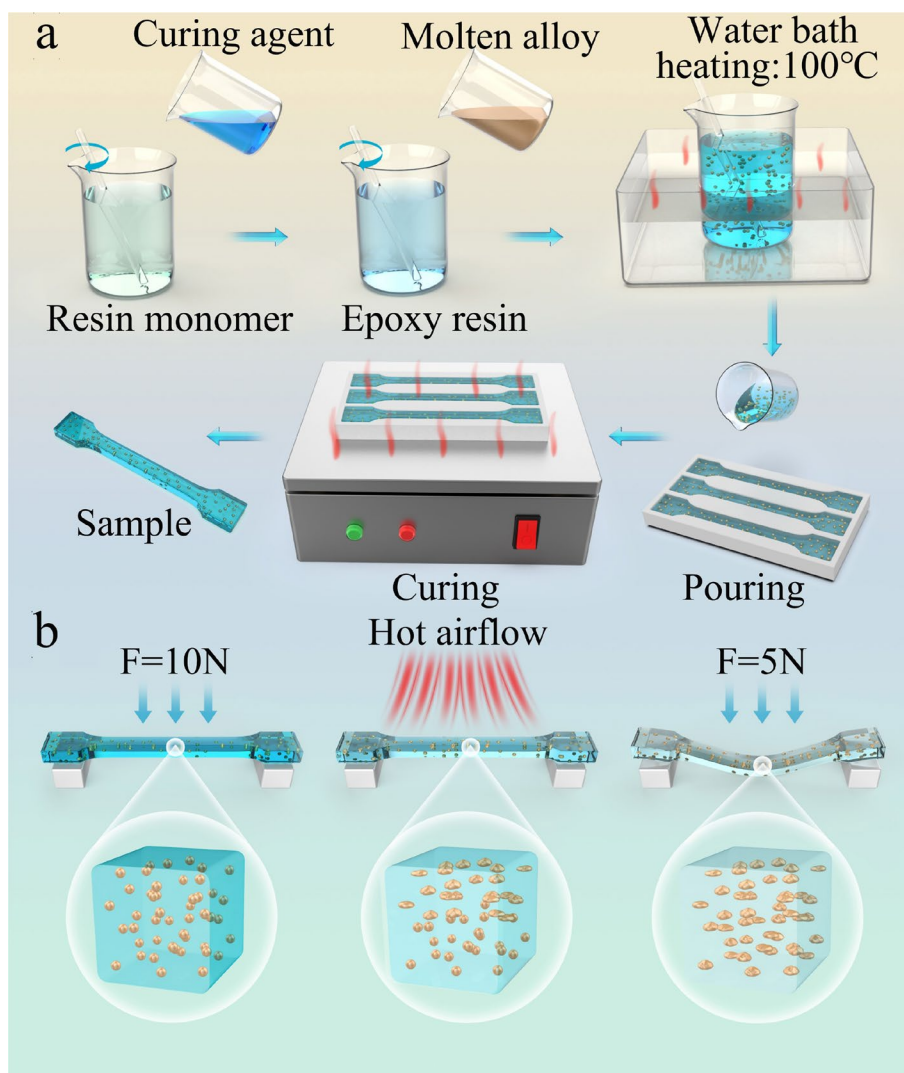
Information). The mixture is stirred evenly in the water bath at 100 °C. Lastly, pouring the well-mixed material into the silicone rubber mold and placing it on a heating platform at 50 °C for at least 12 h. The material is completely cured and demolded to obtain samples with the ability of stiffness variation. The resin cured with EPIKURE3164 has good flexibility and is not particularly stiff at room temperature, which provides better applicability in actuators and wheels.

To investigate the mechanism of stiffness variation of this composite material, we performed differential scanning calorimetry and thermogravimetric analysis (DSC-TGA) tests on epoxy resin, Bi-In-Sn alloy and composite, respectively. The epoxy resin we selected is a thermosetting polymer that forms a mesh structure after curing. DSC results show that the glass transition temperature of the polymer is about 50 °C ($T_g \approx 50$ °C), at which point it changes from a rigid glassy state to a flexible rubbery state. At the same time, a small amount of bisphenol A evaporates during the heating process, so there is a small change in the weight of the resin. The low-melting-point alloy chosen for the experiments, whose main components are Bi-In-Sn (the percentages by weight is 33.5% Bi, 50% In, 16.5% Sn), has a melting point of about 64 °C ($T_m \approx 64$ °C), as determined by DSC experiments. The results demonstrate the effect of both components on stiffness of composite (Figure S1, Supporting Information). As the temperature increases, the epoxy resin gradually softens and the Bi-In-Sn alloy gradually melts. The combined effect of the two changes the stiffness of composite. Its variable stiffness behavior is influenced by the combination of softening of epoxy resin and melting of Bi-In-Sn alloy. The mechanism of stiffness variation is shown in Fig. 1b.

2.2 Material Properties

To investigate the effect of alloy contents on the composites, we observed the tensile sections of the composites with different alloy contents. The cross-sectional shape is shown in Fig. 2a–e. The image results show that the metal particles were well covered by resin matrix in the cross section, but there were also cases of cavitation due to the obvious loss of metal particles. The Bi-In-Sn alloys exist mainly as spherical particles. When the alloy content is small, the particles have a good interface with the substrate (Fig. 2a, b). With the increase in metal content, many particles are exposed and the composite material exhibits brittle characteristic (Fig. 2c). Continuing to increase the metal content, it can be seen that the resin matrix is broken but still in continuous phase (Fig. 2d, e). Although the metal content is large, they are still present in granular form and are encapsulated by resin, which does not form continuous phase. Despite the different Bi-In-Sn alloy content in the composites, the trend of the metal's particle size distribution is similar (Fig. 2f).

Fig. 1 Preparation of variable stiffness materials. **a** The overall preparation process of the material. **b** The variable stiffness mechanism of the composite



As the metal content increases, the overall number of metal particles further increases. The sizes of metal particles are mostly concentrated in the range of 0–10 μm , and a certain number of metal particles exist in other ranges, but the number is very small. Such small alloy particles can be more uniformly distributed in the resin matrix, obtaining better heat transfer and thermal conductivity, and achieving rapid and uniform temperature changes. The particle size distribution of Bi-In-Sn alloy in the resin matrix is obtained by analytical processing of Fig. 2a, e using the color threshold, and particle functions are analysed in the ImageJ software as shown in Fig. 2f. At higher alloy content (40 vol%, 50 vol%), the metal tends to aggregate to produce larger alloy grains, which negatively affects the material properties. There is no necessary connection between the size and volume fraction of alloy particles. In terms of the preparation of low-melting-point alloy particles alone, an aqueous solution containing sodium oleate or sodium dodecyl sulphate and other surfactants can be added to the molten alloy, and

then different stirring speeds are adopted to obtain a mixed suspension of alloy particles and surfactant aqueous solution, followed by a series of processes such as extraction, washing and negative pressure drying to obtain low-melting-point alloy particles of different particle sizes. Moreover, the alloy tends to separate out when the material is in a flexible state (70 $^{\circ}\text{C}$) and bear large loads. These can reduce the reusability of the material. Compared to previously reported stiffness-tunable materials, such as silica sponges filled with molten metal [26] (18-fold change in stiffness) or embedded low-melting-point metals in PDMS [24] (26-fold change in stiffness), our material (when with 30 vol% alloy) allows for a greater range of stiffness variation (tensile modulus changes 41.6 times and compressive modulus changes 58.9 times). Due to the highly inhomogeneous morphology of larger particle sizes, particles with a particle size of less than 400 μm are used in composite manufacturing. Based on the current research work in this paper, for any certain amount of alloy content, in the temperature range of 20–70 $^{\circ}\text{C}$, alloy

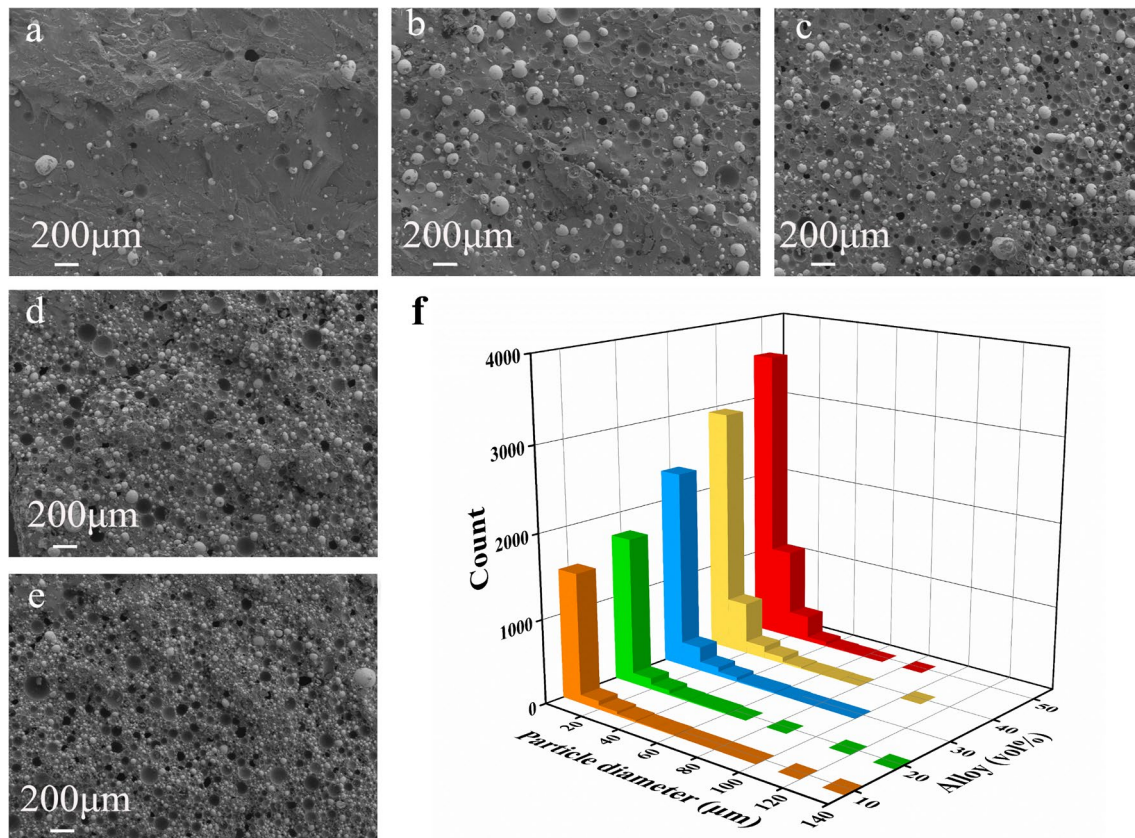


Fig. 2 Tensile cross-sectional micromorphology of composites (with different alloy contents) **a** 10vol% **b** 20vol% **c** 30vol% **d** 40vol% **e** 50vol%. **f** The size distribution of alloy particles

particles with particle size less than 10 μm have less influence on stiffness because of their small volume, while alloy particles with diameter in the range of 10–140 μm account for most of the total volume and have a greater influence on stiffness and can achieve a better range of stiffness variation.

Furthermore, we obtained the stress–strain curves of composites at different temperatures by uniaxial tension and compression experiments (Figure S2–S3, Supporting Information), and its elastic modulus was obtained by calculating. When the Bi-In-Sn alloy content in the composite is 10 vol%, the tensile and compressive modulus of the material is 804.21 MPa and 497.2 MPa, respectively. The stiffness of the composite was further increased with the addition of low-melting alloy content. When the alloy content increases to 30 vol%, the tensile modulus increases to 852.64 MPa and the compressive modulus grows to 530 MPa. As the temperature gradually increases, the resin materials gradually change to rubber state, the stiffness of material decreases significantly (Fig. 3a, b), and the surface hardness gradually reduces (Fig. 3c). Since the curing agent used in the experiment is a polyamide-based epoxy curing agent, which increases flexibility of the resin material, the cured resin also softens before the temperature reaches its T_g . As the

temperature rises to 70 $^{\circ}\text{C}$, the alloy melts completely and the stiffness decreases further. At 70 $^{\circ}\text{C}$, tensile modulus of the composite (alloy content of 10 vol%) is 38.44 MPa and compressive modulus is 20.46 MPa. Compared with the room temperature state, the tensile modulus ratio is 20.9 times and the compressive modulus ratio is 24.3 times. When the alloy content becomes 30 vol%, the material has a tensile modulus of 18.57 MPa and a compressive modulus of 12.47 MPa. The tensile modulus changes 45.9 times and the compressive modulus changes 42.5 times when compared to the room temperature condition. Figure 3d shows the rate of change of tensile and compressive stiffness of composites, respectively, where the cold state is 20 $^{\circ}\text{C}$ and the hot state is 70 $^{\circ}\text{C}$. In addition, the stiffness cycling characteristics of the composites are tested, and the results show that the composite exhibit stable mechanical properties with a good magnitude of stiffness change within 100 thermal cycles, as shown in Fig. 3e. Composites with different alloy contents all exhibit lower stiffness, and the more metal content, the lower stiffness. The results indicate that incorporation of alloys increases the initial stiffness of composites at room temperature while lowering the stiffness limitation after alloy melting, thus extending the range of stiffness variation

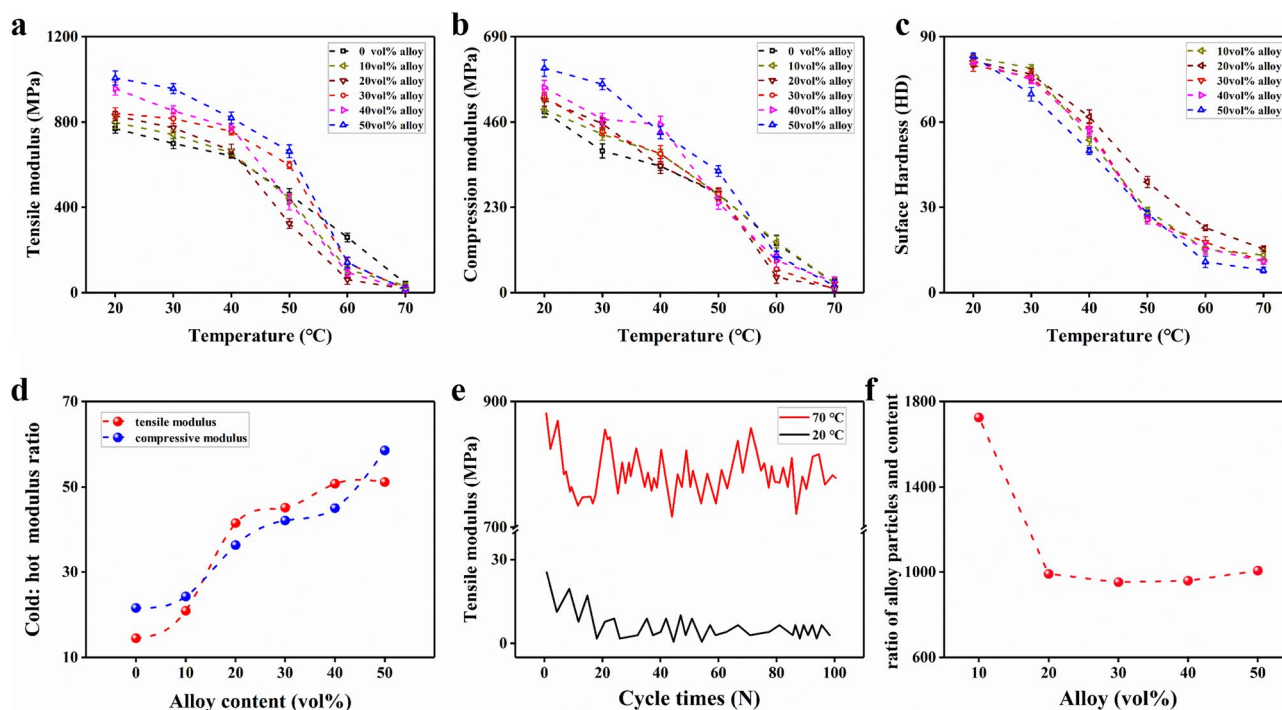


Fig. 3 Properties of composites. **a** Tensile modulus of composites (with different alloy content) at different temperatures, **b** compressive modulus of composites (with different alloy content) at different temperatures, **c** surface hardness of composites (with different alloy content) at different temperatures, **d** cold: hot tensile and compressive

modulus of composites (with different alloy content). Cold condition means 20 °C, hot condition means 70 °C. **e** Stiffness cycling characteristic curve of composite (the alloy content is 30vol%). **f** ratio of alloy particles and content (with different alloy content)

of composites. When the alloy content is 30 vol%, the proportion of alloy particles is lowest, more stable and durable (Fig. 3f). Therefore, the composite system with alloy content of 30 vol% is most suitable in the application.

3 Applications

3.1 Variable Stiffness Pneumatic Actuator

The adjustable stiffness characteristic of composites is similar to the stiffness variation of biological muscles [29]. Its controllability and adaptability to complex environments make it a huge attraction for soft machinery. Here, based on the composites above, we designed and fabricated a variable stiffness pneumatic actuator consisting of three parts: the cavity part, the strain limiting layer and the variable stiffness structure (Fig. 4a). The manufacturing process is shown in Fig. 4b, and the geometric dimensions in Figure S4 (Supporting Information). The cavity section and strain limiting layer are cast with silicone (Dragon skin30). The composite material with 30 vol% alloy is used to build the variable stiffness structural part, which has a serpentine arrangement of nichrome wires ($d=0.3$ mm) on its surface. The three

parts are bonded in sequence using uncured Dragon skin 30 silicone to produce a pneumatic actuator with variable stiffness. It can be powered by air pressure and temperature, which is in striking contrast to conventional air pressure actuation. The resistance wire is evenly arranged inside the composite, and the temperature change of the composite is achieved by Joule heating, which enables accurate control of the temperature change position and improves efficiency to achieve the effect of gradient stiffness. In order to verify the deformation mechanism of this variable stiffness pneumatic actuator, a finite element analysis simulation was performed as shown in Fig. 4c.

Meanwhile, we recorded pictures of the deformation of actuators at specific operating conditions and derived the bending angle and displacement values described in the text by tool measurements and scale calculations. At a constant pressure of 50 kPa, by energizing the resistive wire, the temperature increases from room temperature to 70 °C, resulting in the stiffness variation of composite, allowing the actuator to achieve different degrees of bending. Figure 4e illustrates the tip displacement of the actuator with temperature. When the temperature is in the range of 20–70 °C and the actuator is applied to an air pressure of 50 kPa, the tip displacement increases from 38.1 to 102 mm, expanding by

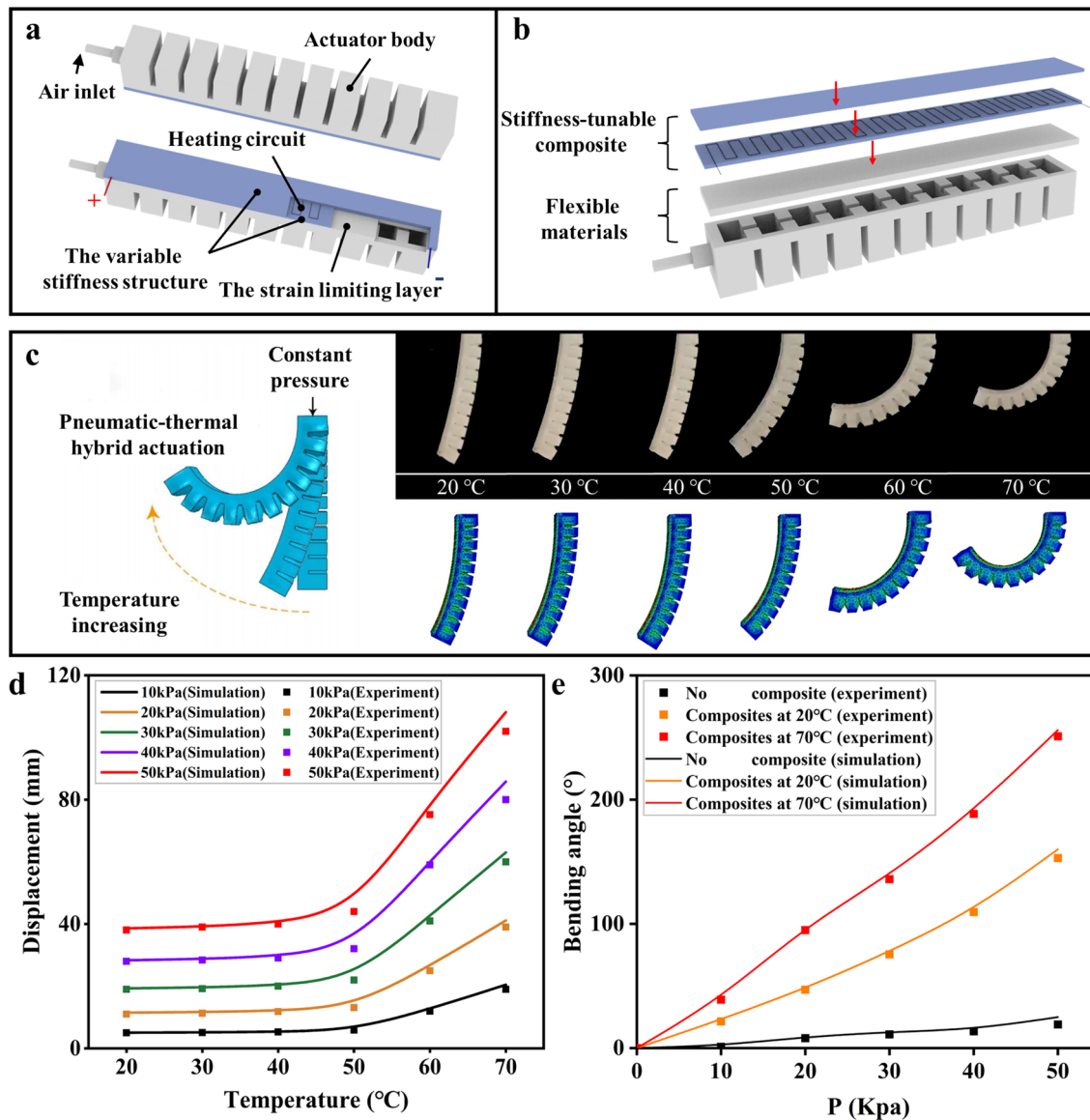


Fig. 4 Deformation effect of variable stiffness actuator. **a** The structure of variable stiffness actuator. **b** The manufacturing process of variable stiffness actuator. **c** Bending deformation and finite element analysis results of the actuator with temperature at 50 kPa. **d** Tip displacement of the stiffness-tunable actuator with temperature. **e** Bending angle of three types of actuators with temperature (pure silicone

pneumatic actuator; pneumatic actuator with 30 vol% alloy content of composites as variable stiffness layer, the variable stiffness layer is in the rigid state; pneumatic actuator with 30 vol% alloy content of composites as variable stiffness layer, the variable stiffness layer is in the flexible state)

2.7 times. The bending angle increased from 19° to 153°, an eightfold increase. And the tip displacement of the actuator shows an exponential increase. The simulated results are in good agreement with the experimental values (Fig. 4d). The results of multiple iterations of the experiment show that the actuator can be operated reversibly through a heat-drive-cool process.

In order to quantitatively study the load capacity of variable stiffness actuators, we constructed a drive force test system (Figure S5, Supporting Information). The force

sensor was fixed on the linear stage, and the displacement sensor was fixed on the horizontal surface. The end of the actuator was fitted with a rigid end to prevent breakage of the actuator due to pushing. During the whole test, the horizontal linear stage moved forward at a speed of 0.5 mm/s, prompting the force sensor to push the rigid end of the variable stiffness actuator, causing the actuator to move [8]. A constraining platform was placed near the cavity side of the actuator to prevent buckling due to the structural instability caused by the tip loading on a pressurized variable stiffness

actuator [30]. We conducted end force tests on three types of actuators: pneumatic actuators with pure silicone; pneumatic actuator with composite materials (the content of alloy is 30 vol%) for the variable stiffness layer, and the variable stiffness layer is in the rigid state (20 °C); pneumatic actuator with composite materials (the content of alloy is 30 vol%) for the variable stiffness layer, and the variable stiffness layer is in the flexible state (70 °C). As air pressure increasing, the initial force at zero displacement increases significantly for all three types of actuators (Fig. 5a–c). At constant air pressure, the force applied to the actuator increases significantly

as the displacement gradually increases from 0 to 5 mm. The force–displacement curves of all three exhibit obvious linear characteristic at air pressures of 25 kPa and 50 kPa. We compared the end forces of the three types of actuators at a displacement of 5 mm (Fig. 5d). When a hard composite layer is used to replace a pure soft silicone layer, the driving force is increased from 137 to 2931 mN at 0 kPa air pressure, which is increased by about 21 times. When an air pressure of 50 kPa is applied, the driving force is increased from 1776 to 4930 mN, which is about three times higher. Under the same conditions, the bending angle of the actuator with the

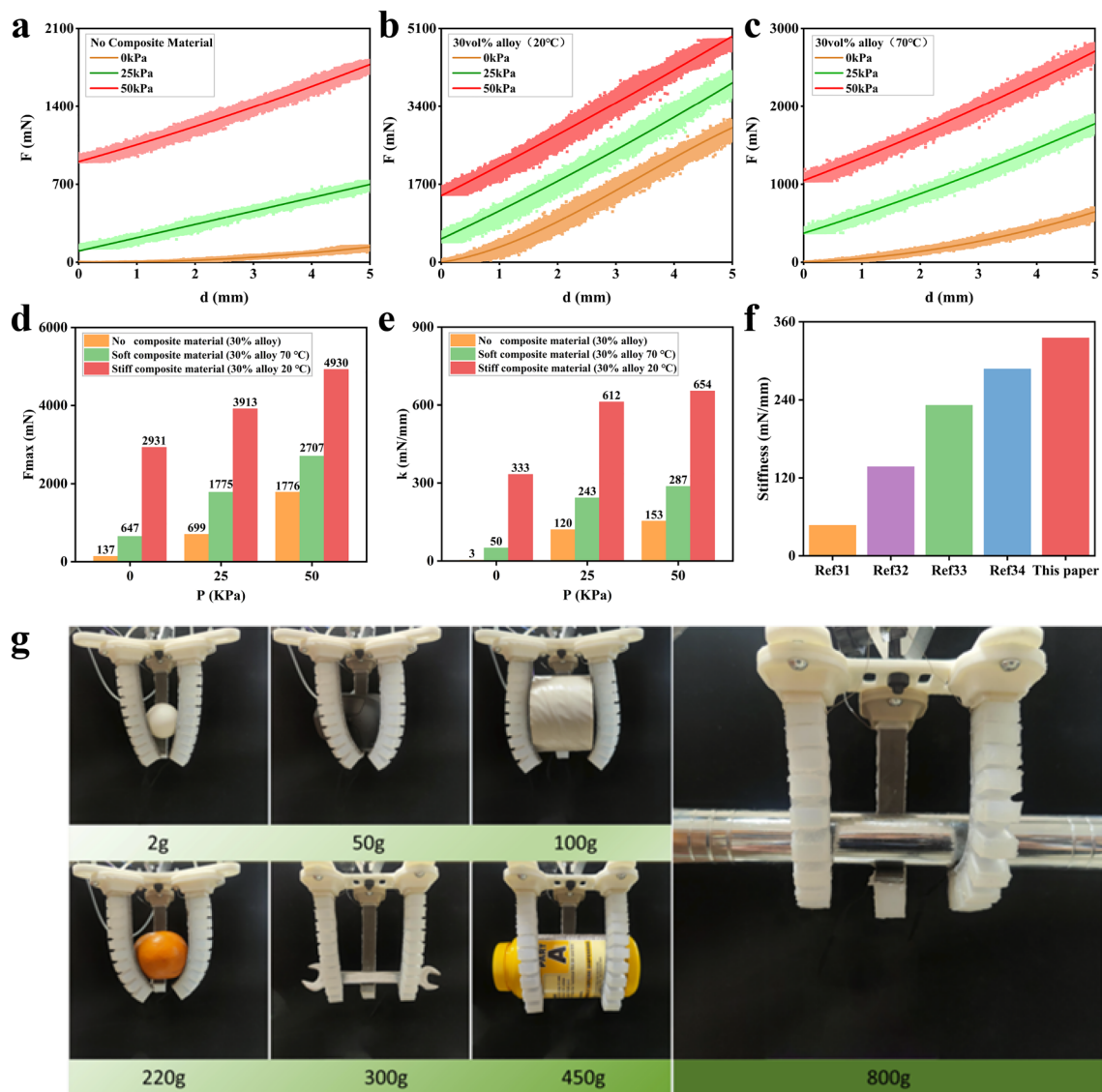


Fig. 5 a–c Tip output force F plotted as a function of tip displacement d on actuator with respect to no composites, stiff composites (20 °C), and soft composites (70 °C) inflated with pneumatic pressures of 0, 25, and 50 kPa, respectively. The measured data are plotted as bands and the curves fitted with a second-order polynomial method are plotted as solid lines. **d** Comparison of maximum output

forces F_{max} in all the tested scenarios. **e** Comparison of initial bending stiffnesses k in all the tested scenarios. **f** Comparison of stiffness with relevant works in the literature. **g** Demonstration of high load capacity and good shape adaptivity by a versatile gripper equipped with three variable stiffness actuators

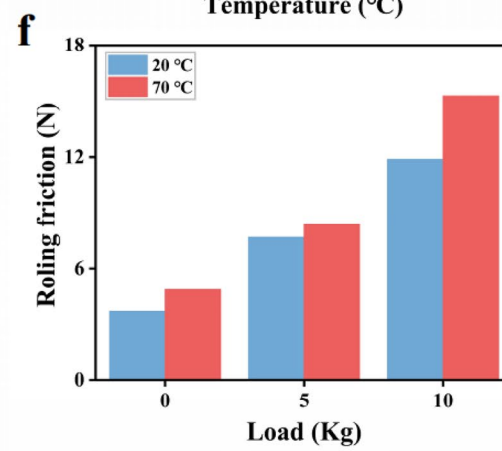
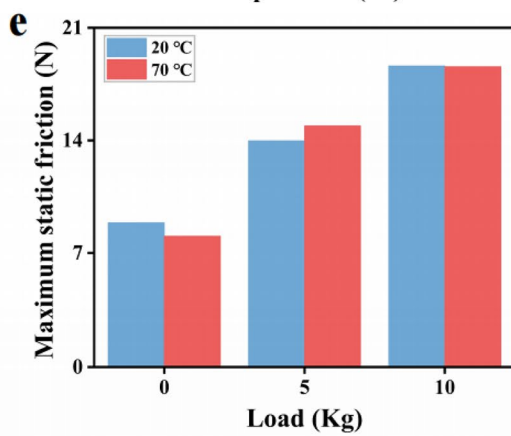
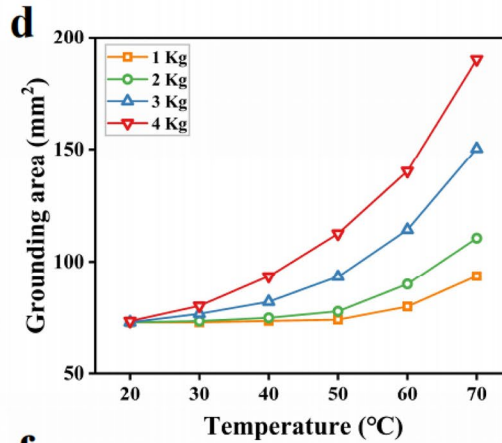
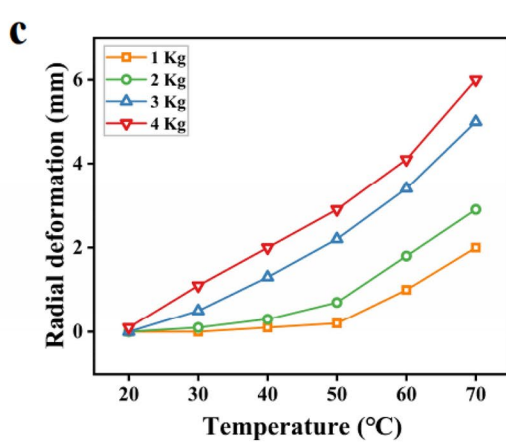
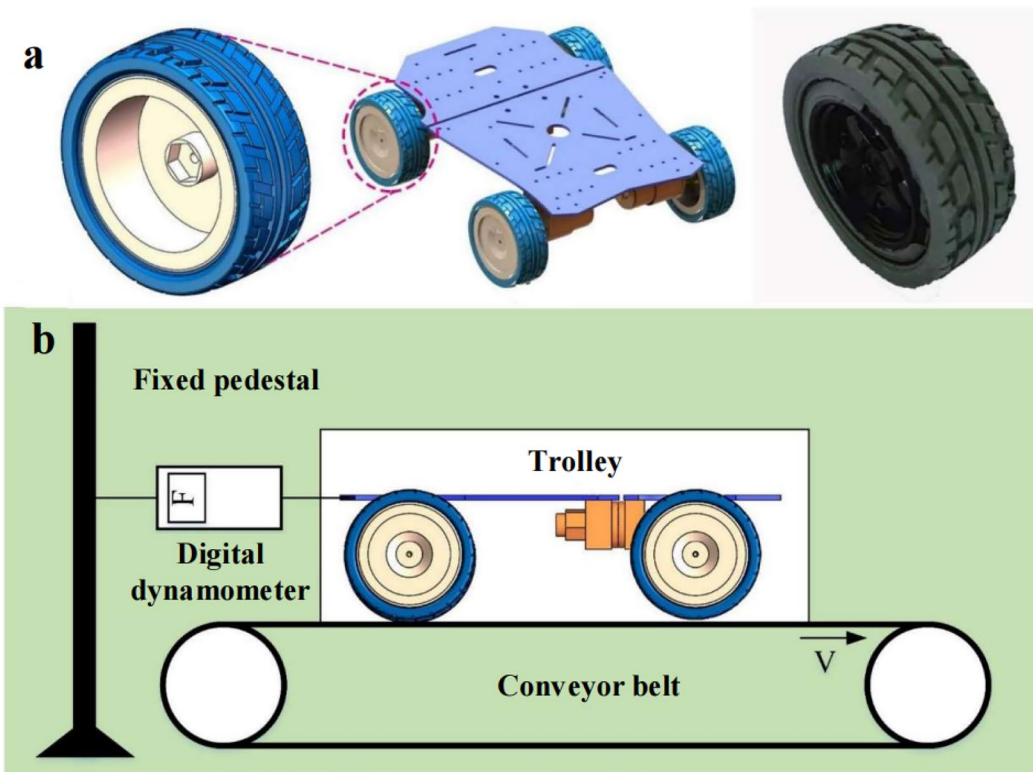


Fig. 6 Friction test and characterization of deformation of stiffness-tunable wheels. **a** Schematic and physical of wheel consisting of stiffness-tunable tread and rigid plastic hub. **b** Schematic diagram of the friction test device. **c** Radial deformation of the tire in the direction of pressure. **d** Grounding area of tire under different conditions. **e** Maximum static friction of tires at different temperatures. **f** Rolling friction of tires at different temperatures

variable stiffness layer in a flexible state is not comparable to that of pure silicone actuator, but it is much larger than the actuator with the variable stiffness layer in a rigid state (Fig. 4e). The bending angle of variable stiffness actuator can reach 153° at an air pressure of 50 kPa after the temperature rises to 70°C . This shows that variable stiffness composites can significantly increase the output force of the actuator without losing its flexibility.

Figure 5e compares the initial bending stiffness of three types of actuators. When the soft silicone layer is replaced by a rigid composite layer, the initial bending stiffness increases by about 124 times at 0 kPa air pressure from 2.69 to 332.96 mN/mm. When 50 kPa air pressure is applied, the initial bending stiffness increases from 152.6 to 653.63 mN/mm, an improvement about 4.3 times. Compared to previously reported SMP-enabled stiffness-adjustable soft actuators [31–34], our stiffness-adjustable actuator has advantage in terms of initial stiffness (Fig. 5f).

In addition, we tested tip output force of variable stiffness actuators with different alloy contents (Figure S6, Supporting Information). When the temperature is 20°C , the composites are in a rigid state. In this instance, tip output force is increased from 1780 to 2931 mN at air pressure of 0 kPa after replacing composites with alloy content of 10 vol% by composites with alloy content of 30 vol%. When a pressure of 50 kPa is applied, the tip output force is increased from 3707 to 4930 mN. After the temperature reaches 70°C , composites with different alloy contents are in the flexible state and the difference in stiffness between them is small. Therefore, the output forces of the actuators do not differ much at this temperature.

In order to further demonstrate the versatility of variable stiffness actuator, we assembled three variable stiffness actuators onto a 3D printed pedestal to develop a gripper with adjustable stiffness. Characteristic of stiffness-tunable makes the soft gripper not only carry heavy loads, but also grasp objects of different shapes and various weights from less than 10–800 g (Fig. 5g). The weight of the actuator is about 100 g. The masses shown in Fig. 5 are 0.02 times, 0.5 times, 1 times, 2.2 times, 3 times, 4.5 times and 8 times the weight of the actuator itself, from small to large.

3.2 Wheel Body with Variable Stiffness

For wheel body material of wheeled wall-climbing robot, traditional designs use homogeneous metals or high molecular

polymer materials. These materials are difficult to change stiffness properties after stable forming and usually do not allow for timely adjustment of complex surfaces. Based on these factors, we designed and manufactured a wheel that consists of hub and tread. The tread has a symmetrically distributed pattern with a filling rate of 94.89%. The wheel hub is made of hard plastic. The tread is made of variable stiffness composites with alloy content of 30 vol% and contains serpentine arrangement of nichrome wires inside. Adjusting the temperature, the stiffness of tire's surface can be continuously changed in multiple steps to accommodate complex surfaces. In this application, the same uniform arrangement of resistance wire inside the composite and Joule heating are used to precisely control the location of temperature changes and improve efficiency.

The wheel structure was prepared by 3D printing technology, and the stiffness-tunable material was poured onto the outer side of wheel to make a wheel with stiffness variation, as shown in Fig. 6a. The prepared variable stiffness wheels were mounted on a four-wheel trolley, and a friction test setup was built. The trolley was placed horizontally on the conveyor belt. A dynamometer was attached to the end of trolley, and the dynamometer was fixed. The wheels were electrically heated, and after the temperature reached the test temperature, the conveyor belt was run at a speed of 1 m/s. The traction force applied to trolley at different temperatures were measured, and the maximum static and dynamic friction were derived from the traction force curve.

As shown in Fig. 6c, d, when a single wheel bears a load of 4 kg, the grounding area is 73.57 mm^2 and the deformation in the direction of pressure is 0.1 mm at the temperature of 20°C . With increasing temperature, radial deformation of tire under constant load gradually increases, and contact area between tire and ground increases significantly. When temperature rises to 70°C , grounding area increases to 190.02 mm^2 , which has been improved by nearly 2.6 times. And the deformation in the direction of pressure is 6 mm, which is 60 times higher. We tested actual motion of the vehicle at different temperatures and loads by installing wheels onto a vehicle and making it move at a speed of 1 m/s (Fig. 6b). We obtained the traction force of the trolley at different temperatures and loads. The maximum static (Fig. 6e) and rolling friction (Fig. 6f) of the vehicle at different temperatures and loads are calculated from the traction force curve. As the load increases, both maximum static and rolling friction forces on the vehicle increase. After increasing the load from 0 to 10 kg, the maximum static friction of trolley changes from 8.92 to 18.6 N and the rolling friction increases from 3.69 to 11.88 N at room temperature. At 70°C , the maximum static friction changes from 6.9 to 18.55 N, and the rolling friction increases from 4.84 to 15.28 N. The results show that the change of wheel stiffness has an effect on the friction of trolley.

4 Conclusions

In summary, this article presents a temperature-controlled stiffness-tunable composite through the concept of bionic drive, which is successfully applied to the design of pneumatic actuator and wheel. The combination of low-melting-point metal with polymer increases the stiffness of polymer material at room temperature. At the same time, the stiffness of polymer material at high temperatures is slightly reduces. The higher the Bi-In-Sn alloy content, the greater the initial stiffness of the composite, and the greater the range of stiffness variation. When the alloy content is 30 vol%, the initial tensile and compressive modulus of composite are 852.64 MPa and 530 MPa, respectively. As the temperature increases to 70 °C, the tensile modulus decreased by 45.9 times and the compressive modulus decreased by 42.5 times. The initial stiffness of pneumatic actuator is up to 332 mN/mm, an improvement of 124 times. For the wheel, the application of composite allows tires to change their ground area at the right time to improve friction. When the load is 4 kg and the temperature is regulated in the range of 20–70 °C, the grounding area of tire can be achieved between 73.57 and 190.02 mm². The rolling friction of trolley increases from 11.88 to 15.28 N when the load is 10 kg. The stiffness-tunable composite based on the bionic drive principle are used to great effect in the field of pneumatic actuators and wheels. We believe that the versatility and applicability of this composite will be proven in an increasing number of application scenarios, which is also the focus of upcoming research.

Supplementary Information The online version contains supplementary material available at <https://doi.org/10.1007/s42235-023-00403-4>.

Acknowledgements This work was supported by the Project of National Key Research and Development Program of China (2018YFA0703300), the National Natural Science Foundation of China (52105299, 52175271, 52021003, 91948302), Science and technology development plan project of Jilin Province (20210509047RQ, 20210508057RQ), Program for JLU Science and Technology Innovative Research Team (2017TD-04).

Author contributions ZL, YL, CL, ZH, and LR conceived the idea and supervised the study. JX and BS carried out the experiments, numerical simulations and analyzed the experimental data. JX, BS, and YL drafted the manuscript, and all authors contributed to the writing of the manuscript.

Availability of date and materials The data that support the findings of this study are not openly available due to some restrictions and are available from corresponding author upon reasonable request.

Declarations

Conflict of interest The authors declare no conflict of interest.

References

- Zhou, P., Yao, J. T., Wei, C. J., Zhang, S., Zhang, H. Y., & Qi, S. P. (2022). Design and kinematic of a dexterous bioinspired elephant trunk robot with variable diameter. *Bioinspiration & Biomimetics*, 17(4), 046016. <https://doi.org/10.1088/1748-3190/ac72e0>
- Yekutieli, Y., Sagiv-Zohar, R., Aharonov, R., Engel, Y., Hochner, B., & Flash, T. (2005). Dynamic model of the octopus arm. I. biomechanics of the octopus reaching movement. *Journal of Neurophysiology*, 94(2), 1443–1458. <https://doi.org/10.1152/jn.00684.2004>
- Ahmed, F., Waqas, M., Shaikh, B., Khan, U., Soomro, A. M., Kumar, S., Ashraf, H., Memon, F. H., & Choi, K. H. (2022). Multi-material bio-inspired soft octopus robot for underwater synchronous swimming. *Journal of Bionic Engineering*, 19(5), 1229–1241. <https://doi.org/10.1007/s42235-022-00208-x>
- Hao, Z. Y., Wang, S., Nie, J. C., Li, D. C., Fang, A. O., Kang, J. F., Liu, C. Z., & Wang, L. (2020). Effects of bionic mechanical stimulation on the properties of engineered cartilage tissue. *Bio-Design and Manufacturing*, 4(1), 33–43. <https://doi.org/10.1007/s42242-020-00090-8>
- Shah, D. S., Yang, E. J., Yuen, M. C., Huang, E. C., & Kramer-Bottiglio, R. (2021). Jamming skins that control system rigidity from the Surface. *Advanced Functional Materials*, 31(1), 2006915. <https://doi.org/10.1002/adfm.202006915>
- Narang, Y. S., Vlassak, J. J., & Howe, R. D. (2018). Mechanically versatile soft machines through laminar jamming. *Advanced Functional Materials*, 28(17), 1707136. <https://doi.org/10.1002/adfm.201707136>
- Lin, Y. Q., Yang, G., Liang, Y. W., Zhang, C., Wang, W., Qian, D. H., Yang, H. Y., & Zou, J. (2020). Controllable stiffness origami “skeletons” for lightweight and multifunctional artificial muscles. *Advanced Functional Materials*, 30(31), 2000349. <https://doi.org/10.1002/adfm.202000349>
- Zhang, Y. F., Zhang, N. B., Hingorani, H., Ding, N. Y., Wang, D., Yuan, C., Zhang, B., Gu, G. Y., & Ge, Q. (2019). Fast-response, stiffness-tunable soft actuator by hybrid multimaterial 3D printing. *Advanced Functional Materials*, 29(15), 1806698. <https://doi.org/10.1002/adfm.201806698>
- Wang, W., Yu, C. Y., Serrano, P. A. A., & Ahn, S. H. (2020). Shape memory alloy-based soft finger with changeable bending length using targeted variable stiffness. *Soft Robotics*, 7(3), 283–291. <https://doi.org/10.1089/soro.2018.0166>
- Kang, J. H., Siochi, E. J., Penner, R. K., & Turner, T. L. (2014). Enhanced adhesive strength between shape memory polymer nanocomposite and titanium alloy. *Composites Science and Technology*, 96, 23–30. <https://doi.org/10.1016/j.compscitech.2014.03.003>
- Wang, X. D., Jian, W., Lu, H. B., Lau, D., & Fu, Y. Q. (2021). Selective entanglement coupling of nanoparticles in polymer nanocomposite with high shape recovery stress. *Composites Science and Technology*, 207, 108728. <https://doi.org/10.1016/j.compscitech.2021.108728>
- Hou, Z. H., Tian, X. Y., Zhang, J. K., Zheng, Z. Q., Zhe, L., & Li, D. C. (2021). Optimization design and 3D printing of curvilinear fiber reinforced variable stiffness composites. *Composites Science and Technology*, 201, 108502. <https://doi.org/10.1016/j.compscitech.2020.108502>
- Jackson, J. A., Messner, M. C., Dudukovic, N. A., Smith, W. L., Bekker, L., Moran, B., Golobic, A. M., Pascall, A. J., Duoss, E. B., Loh, K. J., & Spadaccini, C. M. (2019). Field responsive mechanical metamaterials. *Science Advances*, 4(12), eaau6419. <https://doi.org/10.1126/sciadv.aau6419>
- Song, B. K., Yoon, J. Y., Hong, S. W., & Choi, S. B. (2020). Field-dependent stiffness of a soft structure fabricated from

- magnetic-responsive materials: Magnetorheological elastomer and fluid. *Materials*, 13(4), 953. <https://doi.org/10.3390/ma13040953>
15. Wang, C., Fischer, A., Ehrlich, A., Nahmias, Y., & Willner, I. (2020). Biocatalytic reversible control of the stiffness of DNA-modified responsive hydrogels: Applications in shape-memory, self-healing and autonomous controlled release of insulin. *Chemical Science*, 11(17), 4516–4524. <https://doi.org/10.1039/d0sc01319f>
 16. Zhuo, S. Y., Zhao, Z. G., Xie, Z. X., Hao, Y. F., Xu, Y. C., Zhao, T. Y., Li, H. J., Knubben, E. L., Wen, L., Jiang, L., & Liu, M. J. (2020). Complex multiphase organohydrogels with programmable mechanics toward adaptive soft-matter machines. *Science Advances*, 6(5), eaax1464. <https://doi.org/10.1126/sciadv.aax1464>
 17. Yang, F., Cholewinski, A., Yu, L., Rivers, G., & Zhao, B. X. (2019). A hybrid material that reversibly switches between two stable solid states. *Nature Materials*, 18(8), 874. <https://doi.org/10.1038/s41563-019-0434-0>
 18. Handral, H. K., Natu, V. P., Cao, T., Fuh, J. Y. H., Sriram, G., & Lu, W. F. (2022). Emerging trends and prospects of electroconductive bioinks for cell-laden and functional 3D bioprinting. *Bio-Design and Manufacturing*, 5, 396–411. <https://doi.org/10.1007/s42242-021-00169-w>
 19. Yamada, Y., Iwata, K., Kadowaki, T., & Sumiya, T. (2017). Method of reduced variables for stiffness degradation process of unidirectional CFRP composites subjected to alternating bending. *Composites Science and Technology*, 138, 117–123. <https://doi.org/10.1016/j.compscitech.2016.11.011>
 20. Guilbaud, S., & Audoin, B. (2017). Characterization of temperature-induced stiffness changes in a C-PMR15 composite material by means of laser generated and detected ultrasound. *Composites Science and Technology*, 61(3), 433–438. [https://doi.org/10.1016/S0266-3538\(00\)00095-6](https://doi.org/10.1016/S0266-3538(00)00095-6)
 21. Maples, H. A., Smith, O., Burgstaller, C., Robinson, P., & Bismarck, A. (2016). Improving the ply/interleaf interface in carbon fibre reinforced composites with variable stiffness. *Composites Science and Technology*, 128, 185–192. <https://doi.org/10.1016/j.compscitech.2016.03.028>
 22. Wang, L. Y., Yang, Y., Chen, Y. H., Majidi, C., Iida, F., Askounis, E., & Pei, Q. B. (2018). Controllable and reversible tuning of material rigidity for robot applications. *Materials Today*, 21(5), 563–476. <https://doi.org/10.1016/j.mattod.2017.10.010>
 23. Rothmund, P., Ainla, A., Belding, L., Preston, D. J., Kurihara, S., Suo, Z. G., & Whitesides, G. M. (2018). A soft, bistable valve for autonomous control of soft actuators. *Science Robotics*, 3(16), eaar7986. <https://doi.org/10.1126/scirobotics.aar7986>
 24. Schubert, B. E., & Floreano, D. (2013). Variable stiffness material based on rigid low-melting-point-alloy microstructures embedded in soft poly (PDMS). *RSC Advances*, 3(46), 24671–24679. <https://doi.org/10.1039/c3ra44412k>
 25. Poon, R., & Hopkins, J. B. (2020). Phase-changing metamaterial capable of variable stiffness and shape morphing. *Advanced Engineering Materials*, 21(12), 1900802. <https://doi.org/10.1002/adem.201900802>
 26. Van Meerbeek, I. M., Mac Murray, B. C., Kim, J. W., Robinson, S. S., Zou, P. X., Silberstein, M. N., & Shepherd, R. F. (2016). Morphing metal and elastomer bicontinuous foams for reversible stiffness, shape memory, and self-healing soft machines. *Advanced Materials*, 28(14), 2801–2806. <https://doi.org/10.1002/adma.201505991>
 27. Tonazzini, A., Mintchev, S., Schubert, B., Mazzolai, B., Shintake, J., & Floreano, D. (2017). Variable stiffness fiber with self-healing capability. *Advanced Materials*, 28(46), 10142–10148. <https://doi.org/10.1002/adma.201602580>
 28. McEvoy, M. A., & Correll, N. (2015). Thermoplastic variable stiffness composites with embedded, networked sensing, actuation, and control. *Journal of Composite Materials*, 49(15), 1799–2808. <https://doi.org/10.1177/0021998314525982>
 29. Wang, Y. J., Liu, C. B., Ren, L. Q., & Ren, L. (2021). Bioinspired soft actuators with highly ordered skeletal muscle structures. *Bio-Design and Manufacturing*, 5(1), 174–188. <https://doi.org/10.1007/s42242-021-00148-1>
 30. Sun, Y., Liang, X. Q., Yap, H. K., Cao, J. W., Ang, M. H., & Yeow, R. C. H. (2017). Force measurement toward the instability theory of soft pneumatic actuators. *IEEE Robotics and Automation Letters*, 2(2), 985–992. <https://doi.org/10.1109/LRA.2017.2656943>
 31. Takashima, K., Sugitani, K., Morimoto, N., Sakaguchi, S., Noritsugu, T., & Mukai, T. (2014). Pneumatic artificial rubber muscle using shape-memory polymer sheet with embedded electrical heating wire. *Smart Materials and Structures*, 23(12), 125005. <https://doi.org/10.1088/0964-1726/23/12/125005>
 32. Yang, Y., Chen, Y. H., Wei, Y., & Li, Y. T. (2017). Novel design and three-dimensional printing of variable stiffness robotic grippers. *Journal of Mechanisms and Robotics-Transactions of the ASME*, 8(6), 061010. <https://doi.org/10.1115/1.4033728>
 33. Yang, Y., Chen, Y. H., Li, Y. T., Wang, Z., & Li, Y. Q. (2017). Novel variable-stiffness robotic fingers with built-in position feedback. *Soft Robotics*, 4(4), 338–352. <https://doi.org/10.1089/soro.2016.0060>
 34. Yang, Y., Chen, Y. H., Li, Y. T., Chen, M. Z. Q., & Wei, Y. (2017). Bioinspired robotic fingers based on pneumatic actuator and 3D printing of smart material. *Soft Robotics*, 4(2), 147–162. <https://doi.org/10.1089/soro.2016.0034>

Publisher's note Springer Nature remains neutral with regard to jurisdictional claims in published maps and institutional affiliations.

Springer Nature or its licensor (e.g. a society or other partner) holds exclusive rights to this article under a publishing agreement with the author(s) or other rightsholder(s); author self-archiving of the accepted manuscript version of this article is solely governed by the terms of such publishing agreement and applicable law.